Single-nucleus RNA sequencing reveals the cellular diversity of human cerebrospinal fluid in the context of intraventricular hemorrhage

Sonia Malaiya[1]*, Riccardo Serra[2]*, Marcia Cortes-Gutierrez[1]*, Bradley E. Wilhelmy[2,3], Emily Jusuf[4,5], Mayur Somalinga[4], Dave Peprah[4], Hirschel Nambiar[4], Kevin T. Kim[2], Jordan R. Saadon[2], Parantap D. Patel[2], Steven K. Yarmoska[2], Maureen Rakovec[2], John Kim[2], Catherine Lei[2], Shreyas Panchagnula[2], Reina Ambrocio[6], Meagan Cherney[7], Natarajan Ayithan[8], Xiaoxuan Fan[8], Volodymyr Gerzanich[2], J. Marc Simard[2], Neeraj Badjatia[4,6], Gary Schwartzbauer[2,4], Gunjan Y. Parikh[4,6], Seth Ament[1,9‡], Prajwal Ciryam[4,6‡]

*These authors contributed equally.

‡To whom correspondence should be addressed.

1. Institute for Genome Sciences, University of Maryland School of Medicine, Baltimore, USA.
2. Department of Neurosurgery, University of Maryland School of Medicine, Baltimore, USA.
3. Department of Neurosurgery, The Ohio State University, Columbus, USA.
4. Program in Trauma, University of Maryland Shock Trauma Center, Baltimore, USA.
5. Renaissance School of Medicine, Stony Brook University, Stony Brook, USA.
6. Department of Neurology, University of Maryland School of Medicine, Baltimore, USA.
7. University of Maryland Medical Center, Baltimore, USA.
8. Department of Microbiology and Immunology, University of Maryland School of Medicine, Baltimore, USA.
9. Department of Psychiatry, University of Maryland School of Medicine, Baltimore, USA.

Abstract

Intraventricular hemorrhage (IVH) is a frequent and severe complication of hemorrhagic brain diseases. Treatment options for IVH are limited in their ability to improve long-term functional status. One promising target for treatment is the profound cellular inflammatory response that occurs after injury, but advances have been limited by our incomplete understanding of this phenomenon. We leveraged Recovery After Cerebral Hemorrhage, a prospective, observational study at the University of Maryland, to address this question. We sought to characterize the immune cell populations in the intraventricular cerebrospinal fluid (CSF) of human subjects after IVH. To do so, we generated a single-nucleus RNA sequencing (snRNA-seq) atlas of leukocytes in the CSF after acute brain injury. We performed 10x Genomics snRNA-seq of nuclei isolated from the CSF of 7 patients (ICH=6, SAH=1), yielding 11,191 high-quality transcriptomes. We identified four major cell populations, which we annotated as neutrophils (53.8%), monocytes (26.1%), lymphocytes (17.8%), and other cells (2.4%) based on the expression of canonical gene markers. Sub-clustering revealed distinct subtypes of neutrophils, monocytes, and lymphocytes that shared features with populations previously described in the systemic circulation. Neutrophils were categorized into nascent, quiescent, and interferon-activated states. The interferon-activated state has not been observed in the central nervous system previously. Monocytes were predominantly of a classical phenotype. Lymphocytes were predominantly T-cells, with the largest populations being naïve and central memory $CD4^+$ T-cells. This snRNA-seq data informed the design of a flow cytometry panel that we used to validate the presence of cell subtypes identified by transcriptomics. This analysis demonstrates the feasibility of snRNA-seq approaches to identify previously unexplored pathways and immune cell types that may be relevant to disease. We anticipate that these tools will enable the discovery of new targets to mitigate inflammation-related secondary damage after IVH.

Introduction

Bleeding into the cerebral ventricles, known as intraventricular hemorrhage (IVH), is an ominous complication of hemorrhagic brain diseases, including intracerebral hemorrhage (ICH), subarachnoid hemorrhage (SAH), and traumatic brain injury (TBI). In adults, it results in death or severe disability in over 50% of cases[1]. The development of elevated intracranial pressure and hydrocephalus contribute to morbidity and mortality[2–4]. Treatment options are limited, and around 40% of patients require neurosurgical diversion of cerebrospinal fluid (CSF) using an external ventricular drain (EVD)[5,6]. Ultimately, 20-40% of patients require lifelong shunting of CSF (typically through a ventriculoperitoneal shunt)[7,8]. Though clearance of blood by instilling tissue plasminogen activator into the cerebral ventricles has mortality benefit, it does not clearly improve functional outcomes or reduce the rate of shunting[7]. The placement of a permanent shunt carries long-term risks, including shunt malfunction and meningoencephalitis.

A critical aspect of IVH is the deposition of molecules and cells from the bloodstream into the CSF. These substances stimulate a profound inflammatory response that recruits inflammatory cells into the central nervous system[9,10]. In the first several days after injury, this response is dominated by myeloid cells, first neutrophils, then monocytes/macrophages. These cells collaborate with CNS resident cells, with both pathological and reparative consequences. On one hand, inflammation after IVH can cause neuronal injury, cerebral edema, and hydrocephalus; on the other, it may stimulate neurogenesis and clearance of hemorrhagic debris[11–14].

The role of neutrophils is particularly prominent in the earliest phase of disease. Neutrophils are known to mediate oxidative damage and their depletion in animal models is protective. Until recently, neutrophils were thought to display a relatively limited functional repertoire, owing to their relatively low transcriptional activity and short lifespans. Single-cell RNA sequencing has revealed that, in fact, neutrophils are highly diverse cell populations[15–17,18]. Despite the outsize role that neutrophils play in brain hemorrhage, the small number of single-cell sequencing[19–21] studies that have characterized leukocytes in the central nervous system in human hemorrhagic brain disease have not captured this elusive population of cells.

Here, we sought to characterize the CSF inflammatory response in patients after IVH, using single-nucleus RNA sequencing. Our approach identified distinct states of neutrophils and monocytes in the CSF, including a population of interferon-induced neutrophils not previously described in the central nervous system. These findings illustrate the complex cellular inflammatory response to IVH and point to potential novel therapeutic targets for further investigation.

Materials and Methods

Participants and ethics review.

Subjects (N=7; ICH=6, SAH=1) are a subset of those included in a prospective cohort study of patients aged 18-88 with potentially life-threatening neurologic illness (*NCT04189471*). The University of Maryland, Baltimore, institutional review board (IRB) approved this study, entitled “Improving Outcomes for Patients with Life-Threatening Neurologic Illnesses,” approval: number HP-00056063, date: August 1, 2013. Written informed consent was obtained from subjects (if they had decision-making capacity) or their legally authorized representatives. Study procedures were performed in accordance with the ethical standards of the responsible committee on human experimentation and with the Helsinki Declaration of 1975. Detailed clinical characteristics of study participants were recorded in a secure database, including cytospin cytometry and computed tomography (CT) scans obtained from the participants as part of the standard of care.

Sample preparation and single-nucleus RNA sequencing.

When CSF was aspirated from the proximal port of the EVD during routine clinical practice, excess sample was obtained and transported to the laboratory for immediate processing. *Sample preparation and single-nucleus RNA sequencing. Of the* CSF aspirated from the proximal port of the EVD during routine clinical practice, excess sample was obtained and transported to the laboratory for immediate processing. Obtained CSF was collected on EDTA (purple top vacutainers), with a processing time <1 hour from the time of collection. RNAse and Proteinase/phosphatase were inhibited by adding 1uM DEPC (Sigma D5758) and 1XHALT (Invitrogen 1861281). The cellular component of CSF was obtained by spinning the sample at 350g for 10 min. The pellet was resuspended, and red blood cells were depleted using EasySep magnetic beads (StemCell Technologies cat18170), and Miltenyi microcolumns (Miltenyi cat130-042-701). Samples were then washed and stored at -80C. Half of the samples were stored as pellets and half in cryopreservation media (Cryostor, StemCell Technologies cat 100-1061). All the samples were stored at -80°C in a Mr Frosty for <3 months. For pelleted samples, nuclei extraction was performed directly from the pellets. For samples stored in cryopreservation media, nuclei isolation was performed on the cellular fraction after washing with PBS+1% BSA at 350g/5 minutes at 4C. Nuclei isolation was performed using a detergent-free nuclei isolation kit, Invent (cat IN-024), according to the manufacturer's instructions. Briefly, nuclei were resuspended in buffer A, then vortexed for 20 s at level 9 on Genie2 Vortex, then placed on the spin column at 16000g/30 seconds. The pass-through was washed with buffer B and counted on a MoxiGoII (Orflo) using 1uM Propidium Iodide (Sigma P-4864). We loaded two pools, one pool containing samples stored as pellets and other with cellular fraction cryoprotected. A total of 30K isolated nuclei per pool in PBS+1% BSA were loaded in a 10X Chromium X. Sequencing libraries were prepared by the Maryland Genomics core facility at the Institute for Genome Sciences using Chromium Single Cell 3’ Kit v3.1 reagents, following according to manufacturer’s instructions. Libraries were sequenced on a NovaSeq6000 sequencer (Illumina).

Flow cytometry.

CSF samples were acquired from the EVD buretrol chamber. Samples were stabilized in EDTA tubes during transport from the intensive care unit to the laboratory and kept at room temperature. Samples were then spun at 300g for 5 min, at 4ºC. Pellets were then resuspended in 100 µL of staining buffer (phosphate buffered saline with 1% bovine serum albumin and 1% EDTA - A9418 and 324506, Sigma Aldrich), and incubated for ten minutes on ice with Fc Block (ThermoFisher). Pellets were resuspended in 50 µL of staining buffer mixed with antibodies and incubated for an additional 15 minutes in dark. A 13-antibody panel was used for this experiment. Antibodies included mouse anti-human anti-CD45 (363-0459-41, ThermoFisher), mouse anti-human anti-CD3 (344825, BioLegend), mouse anti-human anti-CD14 (367109, BioLegend), human anti-human anti-CD16b (130-123-643, Miltenyi Biotec), mouse anti-human anti-CD163 (333611, BioLegend), human anti-human anti-CD50 (130-115-309, Miltenyi Biotec), mouse anti-human anti-CD183 (353721, BioLegend), goat anti-human anti-CD121a (FAB269F-025, R&D Systems), mouse anti-human anti-CD62L (567989, BD Biosciences), mouse anti-human anti-CD10 (312241, BioLegend), human anti-human anti-CD181 (130-115-950, Miltenyi Biotec), human anti-human anti-CD182 (130-131-233, Miltenyi Biotec), mouse anti-human anti-CD87 (749063, BD Biosciences). 100 µL of staining buffer were added, cells were mixed and then spun at 300g for five minutes at 4º C. The supernatant was removed, cells resuspended in 200 µL of staining buffer, and 2 µL of 7-amino-actinomycin D (7-AAD) (420404, BioLegend) were added before flow acquisition. Flow acquisition was performed on a Cytek Aurora 4 Spectral Cytometer (Cytek Biosciences, Freemont, CA, USA) at the University of Maryland Greenebaum Comprehensive Cancer Center Flow Cytometry Shared Service. At least 5,000 events were acquired and analyzed with FCS Express V7 software (De Novo Software, Pasadena, CA, USA).

scRNA-seq cell clustering.

Initial data processing was performed with CellRanger (7.2.0), yielding a cell x gene matrix for each pooled sample. Genotype-based demultiplexing was performed with Freemuxlet to group the cells in each pool by genotype. We note that although this approach enables us to evaluate individual variation in cell type proportion, it does not allow us to match genotypes to specific donors. Seurat v4.0.5 was used for batch integration and clustering, using the following parameters. We selected high-quality cells with at least 300 unique molecules and a maximum of 20 percent mitochondrial counts. SCT integration was performed with 5000 variable genes and 20 anchors. Louvain clustering was performed using 20 principal components. An optimal clustering resolution was determined by using the mrtree clustering optimization method, which was given resolutions from 0 to 5, with 3.5 (35 clusters) being optimal for the entire population. Cell clusters were annotated to established cell types based on canonical markers from[22–24]. Subsequently, the most abundant major cell types — neutrophils and monocytes — were sub-clustered, following the same procedures starting from the SCT integration step. Subtypes were compared to neutrophil and monocyte diversity that has been described by scRNA-seq in other contexts. Cells in our snRNA-seq dataset were scored using the combined expression of marker genes from comparison datasets with the AddModuleScore() function in Seurat. Genes from reference datasets were selected with a $\log_2 FC > 0.585$ (greater than 1.5 fold change) and adjusted p-value < 0.05.

Gene co-expression networks in neutrophils and monocytes.

Gene co-expression modules were identified through k-means clustering of imputed read counts, as previously described[25] . First, we performed a zero-preserving imputation with ALRA to reduce dropouts and improve correlation structure. Next, we performed k-means clustering (parameters). Clusters with tightly correlated centroids were merged, and genes with insufficient correlation to the centroids of the merged clusters were dropped. These steps were performed using the cells from Pool 2, then projected onto the cells from Pool 1. This strategy reduces the potential for batch effects during clustering and provided an independent test set to evaluate the robustness of the modules.

Label Transfer in T-cells

The subset of lymphocytes (cells labelled as “B”, “CD4 T”, “CD8 T” and “other T”) from a larger human peripheral blood cell dataset[26] was used to label the subset of lymphocytes from our dataset. We used the CCA method to integrate our data with the reference data through the FindTransferAnchors() and TransferData() functions from Seurat v4.0.5. The CSF nuclei were then mapped into the reference UMAP for visualization.

Results

A snRNA-seq atlas for cellular diversity of ventricular CSF in the context of intraventricular hemorrhage.

Previous scRNA-seq studies of CSF samples from patients with IVH did not capture its full cellular diversity. This is most likely due to the sensitivity of neutrophils and other fragile populations during sample processing. We reasoned that single-nucleus RNA sequencing (snRNA-seq) could provide a means to limit these processing-induced biases of scRNA-seq and might yield a more representative cellular atlas of IVH.

We obtained ventricular CSF of seven study participants who presented with IVH, either directly to the University of Maryland Medical Center or after emergent transfer from another institution (**Fig. 1A**; **Table 1**). Six subjects presented after ICH, with etiologies including hypertension and coagulopathy/anticoagulation-related hemorrhage, with one subject whose etiology was unknown. One subject presented with aneurysmal SAH. Of the seven subjects, five presented with severe deficits in level of consciousness as quantified by Glasgow Coma Scale (GCS) between 3-8 and two presented with a mild deficit (GCS 13-15). Standardized scales of disease severity were consistent with moderate to severe disease. For subjects with ICH, hemorrhages originated in deep structures of the brain in a majority of cases. All subjects had IVH, either at presentation or subsequently in their hospital course. When CSF is obtained for clinical purposes, excess fluid that would otherwise be discarded is sometimes available. We collected this CSF immediately after it was aspirated. As these are convenience samples, they were obtained at a range of time points after disease onset. Non-contrast CT scans of the head from these subjects demonstrate the presence of IVH and show the EVD tip in the lateral ventricles near the foramen of Monro (**Fig. 1B**). CSF is therefore sampled directly from the ventricles, unlike lumbar puncture, which samples CSF from the lumbar cistern in the lower back. CytoSpin cytology data obtained from five of the seven patients indicated extensive infiltration of leukocytes into the CSF, primarily comprised of neutrophils, monocytes/macrophages, and T cells (**Fig. 1C**).

snRNA-seq of CSF from these seven study participants yielded 11,191 high-quality nuclear transcriptomes (**Fig. 2A, B**). Neutrophils (n = 6,017; *S100A8*$^+$, *CXCR1*$^+$, *FCGR3A*$^+$, *FCGR3B*$^+$) were the most abundant, followed by monocytes (n = 2,920; *VCAN*$^+$, *CXCL8*$^+$, *CCL2L1*$^+$), and lymphocytes (n = 1,990; *CD247*$^+$) (**Table S1**). We also identified a small number of cells expressing glial and neuronal markers (n = 264; e.g., *PTPRD, RSPO3, FLT1, CLDN10, RYR2, RBFOX1, DLG2*) (**Fig 2C**). These cells may derive from damage to the cerebral grey matter during or after the placement of the EVD and were not analyzed further. Cell type proportions identified by snRNA-seq were in the same range as those obtained using cytospin columns (**Fig. 1C**), although our pooling strategy does not allow us to match individual samples across the two technologies. Overall, our data represents a relatively unbiased atlas for the cellular diversity of the CSF in the context of IVH.

Participants' cells were preserved for snRNA-seq processing by two different methods, comparing distinct cell processing protocols in which nuclei were isolated directly from frozen cell pellets vs. cells that had been cryopreserved with DMSO and briefly thawed. snRNA-seq of nuclei derived from pelleted vs. cryopreserved cells yielded a larger number of nuclei from the cryopreservation method, but this method also produced lower RNA counts per nucleus and higher mitochondrial counts per nucleus (**Fig. 2B, Fig. S1 A-C**). The library derived from cryopreserved cells contained a smaller fraction of neutrophils and larger fraction of lymphocytes. It is unclear whether these differences correspond to biological variation among the participants, or whether they reflect a greater vulnerability of neutrophils during cryopreservation and thawing. Regardless, these data suggest that all of the cell types in the CSF can be obtained for snRNA-seq by either cell processing strategy.

Neutrophil diversity in the ventricular CSF

Next, we sought to characterize leukocyte subtypes in greater detail. Re-integration of the 6017 nuclei identified as neutrophils identified eight transcriptionally-distinct sub-clusters. All eight sub-clusters were detected in both preservation methods (**Fig. S2A-C**), but with varying proportions. We annotated these neutrophil sub-clusters via comparisons to scRNA-seq of neutrophil states in the blood and in the lumbar CSF[16], enabling us to merge the eight clusters into three broad neutrophil subtypes. As expected, the majority of neutrophils form a continuum from nascent neutrophils (neu 4, neu6, neu8), marked by *S100A8*, *S100A9*, and *SELL*, to quiescent states (neu1, neu2, neu5 and neu7), which expressed markers such as *MALAT1* and *CXCL8* (**Table S2**). In addition, a third population expressed genes that are activated during interferon responses (neu3), including *IFIT1*, *IFIT2*, *IFIT3*, and *FCGR3B*. Interferon-activated neutrophils are a sub-population with diverse but not fully characterized functions[27,28]. Notably, they have never been described in the CSF previously.

We further quantified these neutrophil subtypes by scoring each population in our dataset on the combined expression of the marker genes from neutrophil subtypes in a published scRNA-seq atlas of circulating neutrophils in human blood[16] (**Fig. 3B, Table S4**). This analysis confirmed that, consistent with Franco and colleagues, the markers for the Nh0 "immature" neutrophils had significantly greater expression in our nascent neutrophils (ANOVA p-value < $2*10^{-16}$; detailed post-hoc statistical analysis is shown in **Table S8**). The Nh1 "transitional phenotype" markers are expressed across all neutrophils in our data with relatively minor

differences between the three subtypes. In the original classification in circulating neutrophils, Nh1 had the least transcriptionally distinct signature and accounted for the majority of cells. It is therefore not surprising that we saw markers related to Nh1 broadly expressed in the neutrophils we detected in CSF. The Nh2 "transcriptionally inactive" neutrophil markers have low expression throughout our data, but show minor yet significantly higher expression in the quiescent cluster (ANOVA p-value < $2*10^{-16}$) (Fig. 3B). The Nh3 "IFN inducible" markers had significantly higher expression in the interferon activated neutrophils in our data (ANOVA p-value < $2*10^{-16}$). These observations demonstrate the robustness of our classification and suggest that neutrophils in CSF after IVH share functional states with those present in the circulation under normal conditions.

We also scored our cells on the basis of the top 50 most up regulated marker genes from a sepsis-derived whole blood single-cell multiomic study[29] (**Fig S3A, Table S4**). Consistent with our markers for the clusters, we found a statistically significant up regulation of the S100A8-9^{hi} neutrophils markers in all the clusters contributing to our nascent population (ANOVA p-value < $2*10^{-16}$). As expected, the IL1R2+ Immature neutrophil markers were significantly up-regulated in Nascent neutrophils as well (ANOVA p-value < $2*10^{-16}$), and the Quiescent and Interferon-activated subtypes were up regulated for markers of the Mature neutrophils population (ANOVA p-value < $2*10^{-16}$).

To characterize gene modules active in each neutrophil state, we next used gene co-expression network analyses (**Fig. 3C, Fig. S4A, Table S3**). Among 12 gene modules, 3 displayed distinct patterns of activity across neutrophil states. Module M8 was up-regulated in interferon-activated neutrophils (ANOVA p-value < $2*10^{-16}$). Its hub genes included many canonical interferon-stimulated genes (ISGs), including *IFI6, IFI30, IFI44*, *IFI44L, IFIT1, IFIT2* and *IFIT3*, further supporting that these neutrophils mount a robust interferon response. This module consisted of several other genes annotated as being expressed in response to symbionts, viruses, cytokines, and interferons (e.g., *MX1, IFITM3, IFIT5, IFI6, CD74, CXCR4, SELL*) (GO:0140546, GO:0051607, GO:0034097, GO:0034341, GO:0034340, GO:0035456).

Module M7 was up-regulated in a subset of the nascent neutrophils (ANOVA p-value < $2*10^{-16}$). This module's hub genes included several genes involved in the regulation of cell adhesion and cell migration (*CD177, CD44, ITGAM*, and *MME*). It also includes many genes annotated for transcription factor activity (*IL18RAP, CFLAR, TLR4, TRIM25, TLR5, HCK, CR1, MAPK14, SAMSN1*) (GO:0051092, GO:0051091), signaling pathways (GO:0002221, GO:0002224, GO:0019221) and immune responses (GO:0050727, GO:0042116).

Module M12 was highly expressed in both nascent and senescent neutrophils and had low expression in the interferon responsive population (ANOVA p-value < $2*10^{-16}$). Its hub genes included NAMPT, which has been shown to play a significant role in neutrophil development and is suppressed by type I interferons[30], as well as *ADAM8, CD55, JUNB*, and other genes with diverse roles in the inflammatory and migratory states of neutrophils such as phagocytosis (*RAB31, SLC11A1, FPR2, NOTCH1, MYADM, PPM1F*) (GO:0050766), negative regulation of adhesion (GO:0022408, GO:0010810, GO:2000048) and regulation of innate immune response (GO:0045088).

Monocyte diversity in the ventricular CSF

We performed equivalent analyses to characterize monocyte diversity in ventricular CSF (**Fig. 4**). Sub-clustering of the 2,920 monocytes identified 6 transcriptionally distinct clusters, designated Mono1-Mono5 and Mac) (**Fig. 4A, Fig. S5A-C, Table S5**). We further characterized these clusters of monocytes/macrophages based on their expression of canonical marker genes and comparison to publicly available gene expression data for monocyte/macrophage clusters in the MoMac data set[31] (**Fig. 4B, Fig. S6A, Table S7**).

Using this approach, we were able to associate our monocyte/macrophage clusters with established functional states of these cell types. Four of the six clusters exhibited gene expression hallmarks of classical monocytes. Mono1 (36.68%) expressed a few classical monocyte markers[32] such as *CD163, CSF3R, S100A8* and *S100A9*. Mono2 (36.1%) expressed other pro-inflammatory markers also associated with classical monocytes, such as *S100A12, ALO5XAP*, while also expressing markers similar to the interferon-activated neutrophils (*CXCR2, FCGR3B*). Mono3 (15.24%), too, expressed pro-inflammatory markers, which are usually found in response to inflammatory signals, such as *CXCL8, CCL3, CCL4* and *NFKBIA*. Comparing these clusters with those of CD16^{-} MoMac clusters enabled us to better identify features that correspond to classical monocytes. MoMac Cluster 8 is a CD16^{-} cluster that showed differential expression between our monocyte/macrophage clusters (ANOVA p-value < $2*10^{-16}$). Markers of this cluster were significantly up-regulated in the Mono 1, Mono2, and Mono3 nuclei. Markers of the MoMac CD16^{-} cluster 15 (the "IL1B" cluster) significantly higher in clusters Mono 2, Mono3, and Mono5, than in the other clusters. Mono5 (2.53%) also expressed activated monocyte markers such as *CXCL3, CXCL5* and *SERPINB2*. These observations provide further evidence that Mono1, Mono2,

Mono3, and Mono5 exhibit features of classical monocytes, albeit in some cases in an activated state. Mono4 (4.21%) is likely a cluster of intermediate monocytes, as its nuclei expressed MHC class II markers such as *CIITA, HLA-DRA, CD74*, and other intermediate monocyte specific genes. We also found significantly higher expression of the MoMac cluster 14 markers (most of which were MHC Class II genes) in the Mono4 nuclei (ANOVA p-value $< 2*10^{-16}$), which is identified in their dataset as a DC contamination. However, our Mono4 nuclei did not express any canonical dendritic cell markers. The MoMac cluster 3 macrophage markers were more highly expressed in our Mac nuclei (ANOVA p-value $< 2*10^{-16}$), confirming that this is a macrophage cluster.

We used gene co-expression modules generated from monocytes and correlated those with the cell states discovered in our clustering (**Fig. 4C, Fig. S7A, Table S7**). Of the 14 modules generated, we found Module 2 contained genes that were annotated as response to cytokine stimulus (GO:0071345) and general inflammatory responses (GO:0006954, GO:0042116, GO:0050727). This module also contained several ISGs and had significantly higher expression in Mono2 and Mono3 (see **Table S8** for details of statistical significance testing by ANOVA and post-hoc TukeyHSD). Module 6 was expressed by pro-inflammatory cells and contained MHC class 1 genes such as *HLA-A, B* and *C* (GO:0002484, GO:0002476).

The prominent expression of both specific chemokines and their cognate receptor imply a functional relationship between cell clusters. *CXCL3, CXCL5, and CXCL8* are CXCL chemokines and neutrophil chemoattractants that all act through the receptor *CXCR2* (*CXCL8* is also a ligand for the similar receptor *CXCR1*). This may indicate intercellular communication between the Mono3/Mono4 clusters and the Mono2 cluster, as well as the neutrophil clusters in which *CXCR2* is also expressed.

T-cells and non-immune cell diversity in the intraventricular CSF

The nuclei identified in our data as lymphocytes expressed canonical pan-lymphocyte and T cell markers, including *PDE3B*, *FOXP1*, *MBNL1*, *ANK3*, *BCL2*, *FYN*, *SKAP1* and *CD247*. However, we detected expression of B-cell markers (*CD19*, *CD20*, *CD21*) in only a small population of cells, consistent with observations for intraparenchymal hematoma and CSF in subarachnoid hemorrhage by flow cytometry[33,34]. Because of the smaller population of nuclei, we found that our initial clustering methods did not reveal obvious biologically relevant clusters. Therefore, to better characterize lymphocyte populations, we performed a label transfer analysis by integrating our lymphocytes with those from a large PBMC reference atlas and projected our data onto the UMAP from the reference data to identify shared marker genes and confirm annotations[26] (**Fig. 5**). This analysis suggested that most of the lymphocytes we detected are $CD4^+$ central memory T-cells, $CD4^+$ naïve T-cells, $CD8^+$ effector memory T-cells, or $CD4^-CD8^-$ T-cells. It is intriguing that the majority of T-cells we detect are $CD4^+$, particularly naive and central memory $CD4^+$ T-cells. Further sub-clustering of these nuclei showed a population of cells expressing the pro-inflammatory markers also seen in neutrophils and monocytes (CXCR2, S100A8-9, CSF3R, IFITM2). While CXCR2 is most commonly expressed by myeloid lineage leukocytes such as neutrophils, it is also expressed by γδ T-cells[35].

Development of a flow cytometry panel for neutrophil and monocyte diversity in the ventricular CSF

Our snRNA-seq data suggest that specific immune cell subtypes are enriched in the CSF of IVH patients compared to their prevalence in other contexts. Monitoring the abundance and dynamics of these immune cell subtypes could potentially reveal biomarkers that predict clinical outcomes. However, snRNA-seq is not a practical method to track these populations in clinical settings. Leveraging our snRNA-seq data, we sought to develop a panel of cell surface markers to distinguish neutrophil and monocyte subtypes by flow cytometry.

We therefore developed a flow cytometry panel to delineate functional states of neutrophils and monocytes, the two most common cell types observed in our snRNA-seq data. To leverage the insights of our snRNA-seq data, we derived this panel empirically from our data set, as opposed to relying on existing cytometry-based classifications. After identifying cluster of differentiation (CD) genes enriched in specific clusters, we used FluoroFinder (Broomfield, CO) to select a subset of markers for which reliable antibodies with compatible fluorophores existed.

Using this panel, we performed flow cytometry analysis of CSF samples on three samples from two participants with IVH not included in the snRNA-seq analysis. Both participants had experienced thalamic ICH with IVH, one as a result of hypertension and other as a result of a ruptured arteriovenous malformation. As expected, CD45+ immune cells could be distinguished as granulocyte, monocyte, and lymphocyte populations using CD3 and CD14 gating, which were further confirmed by forward and side scatter profiles (**Figure 6A**). Based on neutrophil clustering from our snRNA-seq data, we hypothesized that three canonical neutrophil

surface markers—CD10, CD62L, and CD16b—could help resolve distinct neutrophil subsets[36] . The dominant population (>90% of neutrophils) was $CD10^{+}CD62L^{+}CD16b^{high}$, consistent with mature circulating neutrophils.

CD10 presented a particular interpretive challenge: while transcriptional data, including our own and that from Wigerblad et al.[16], suggest CD10 as a marker of nascent neutrophils, it is better established as a surface protein associated with mature neutrophils. Consistent with this, we observed a small population of $CD10^{-}CD62L^{+}CD16b^{high}$ neutrophils (<2%) consistent with a nascent phenotype, but no $CD10^{+}CD62L^{+}CD16b^{high}$, as otherwise might have been inferred directly from our transcriptomic data **(Figure 6B)**. From our transcriptomic data, we would infer that quiescent neutrophils are $CD10^{-}CD62L^{-}CD16b^{low}$. However, we again anticipated that the protein-level expression of CD10 would differ for these cells, and that quiescent cells should be $CD10^{+}CD62L^{-}$ $CD16b^{low}$. Though both populations are small, the $CD10^{+}CD62L^{-}$ $CD16b^{low}$ population is much more common in our flow cytometry data than is the $CD10^{-}CD62L^{-}$ $CD16b^{low}$ population **(Figure 6B).** A distinct subset of a $CD10^{-}CD62L^{-}$ population is $CD10^{-}CD62L^{-}$ $CD16b^{high}$. Cross-referencing with our snRNA-seq data, this population is most consistent with interferon-activated neutrophils, though the markers shown here do not directly test for that state. Additionally, we identified by flow cytometry a $CD10^{+}CD62L^{-}CD16b^{+}$ subset not resolved in our snRNA-seq clustering analysis but reported in the literature as T cell–suppressive neutrophils[37]. Similarly, we hypothesized that monocyte subtypes could be distinguished using the markers CD163, CD62L, CXCR1, CXCR2, CD50, and CD87. We found that of these, CD163, CD62L, and CXCR1 were the only markers with discriminating power in our flow cytometry data set **(Figure 6C**)**.**

We note that we detect nascent, quiescent, and interferon-activated populations—which together dominate the snRNA-seq neutrophil profile-- at very low levels in our flow cytometry data. It is unclear whether this arises from greater sensitivity of snRNA-seq; misclassification by snRNA-seq due to mismatch between gene and protein expression; limitations of the flow cytometry panel; or patient-specific differences in neutrophil subtype. Taken together, however, our flow cytometry results indicate that it may be possible to translate leukocyte functional states inferred from single-nucleus transcriptomics into clinically-feasible flow cytometry panels.

Discussion

In this study, we generated a single-nucleus transcriptomic atlas of the ventricular CSF in IVH. We leveraged nuclear extraction as a strategy to enrich for cell types — specifically neutrophils — that are often challenging to capture in single-cell experiments because of their fragility. Our results reveal a diversity of cell types, including distinct subpopulations of neutrophils, monocytes, and lymphocytes. Notably, we capture a large and diverse population of neutrophils, including a population of interferon-responsive neutrophils that has not been described in the central nervous system previously. As single-nucleus RNA sequencing is not feasible for clinical diagnostic purposes, we validated potential flow cytometry markers for cellular sub-clusters we identified. This demonstrates the feasibility of translating biomarkers derived from snRNA-seq data into clinically practical flow cytometry markers.

The detection of a large population of neutrophils in the CSF in our study is consistent with cytological data available for five out of the seven subjects. This is a strength of our study that distinguishes it from the existing literature. Our findings contribute to a small but growing body of literature reporting single-cell data after brain hemorrhage. Sansing and colleagues reported single-cell RNA sequencing data from the intraparenchymal hematoma of a patient who underwent clot evacuation after an intracerebral hemorrhage as part of the MISTIE III phase III clinical trial[19]. Their study provides a rich time-dependent atlas of leukocytes in the intracerebral hematoma, including populations of monocytes/macrophages, lymphocytes, NK cells, dendritic cells, neurons, and granulocytes/neutrophils. Because they subjected samples to a specific granulocyte depletion, only a small population of neutrophils is detected either in the hematoma or the peripheral blood. Similarly, the two reported single-cell studies of CSF in subarachnoid hemorrhage[20,21] specifically selected against neutrophils, one profiling PBMCs and the other profiling $CD8^{+}CD161^{+}$. Neutrophils are expected to be among the most common leukocytes present in the first several days after hemorrhage. Therefore, understanding the diversity of their functional states is critical to a comprehensive view of central nervous system inflammation after brain hemorrhage. Our study, therefore, adds valuable new insights about neutrophils in IVH.

Neutrophils may be particularly challenging to capture in single-cell studies. They are short-lived and highly sensitive cell types, rendering them difficult to capture with methods that have long or complex workflows. This raises the question of why we were able to identify a large population of neutrophils when others have not. We analyzed CSF instead of parenchymal hematoma, and these may have different cell populations. However, many neutrophils have been isolated from similar samples by flow cytometry[38]. It is more likely, then, that differences in our sample preparation account for the preservation of neutrophils. The use of single-nucleus instead of single-cell RNA sequencing may improve the identification of neutrophils, as all cells undergo lysis, reducing the bias against fragile neutrophils. While we cannot fully exclude the possibility that the nuclei we

identify as deriving from neutrophils actually arise from other cell types, the expression of canonical neutrophil markers in these cells supports their assignment to this cell type.

A strength of single-nucleus RNA sequencing over traditional cytometric approaches is the ability to distinguish subtle cellular phenotypes and activation states. The advent of these methods has revealed that neutrophils, previously thought to be a relatively homogenous cell type, in actuality exhibit a variety of states. In this case, we identified three major neutrophil functional states, though we anticipate that with larger sample sizes and improved isolation techniques, it is likely we would be able to classify these states even more specifically. We have shown that these are consistent with classifications of neutrophils derived from peripheral blood in independent data sets[16,29].

One particularly interesting neutrophil state is the interferon-activated neutrophil. Interferons have been known to stimulate neutrophils for nearly half a century[39]. Knockout of the Type I interferon receptor results in increased neutrophil accumulation in infected tissue[40,41], while interferon-gamma decreases neutrophil accumulation in such tissue[42] . Interferon-responsive neutrophils also have been shown to play an important role in tumor control[27,43] and the response to SARS-CoV-2 infection[28]. To our knowledge, this subtype of neutrophils has never been reported in the central nervous system previously. Its implications for the pathophysiology of intracerebral hemorrhage are unknown but merit further investigation. This represents a potentially targetable pathway for modulating neutrophils for future therapies.

Our data also reflect a diversity of monocytes/macrophages that occupy a range of functional states. An interesting observation is the expression of ligand-receptor combinations, such as CXCL8 and CXCR2, that may indicate cross-talk between subtypes with a cell type (e.g., Mono2 with Mono3) or between cell types (e.g., Mono2 with interferon-activated neutrophils). We also observed monocyte/macrophage phenotypes that have been associated with disease. For example, both snRNA-seq and flow cytometry a substantial number of $CD163^{+}$ monocytes/macrophages, a population that has been associated with disease severity in aneurysmal subarachnoid hemorrhage[44].

The distribution of lymphocytes we observed in the CSF is intriguing and merits further investigation. It has been reported that the majority of T cells in the CSF under normal conditions exhibit a central memory phenotype[45]. This was one of the major subtypes we observed in IVH, though not the most common. These cells have been purported to enter the CSF via the choroid plexus[46].

Limitations of our study include a small sample size and insufficient material for genotyping, both of which reduce our ability to delineate differences inflammatory profiles that are associated with disease severity. These samples were convenience samples that were obtained when specific clinical events (EVD placement, EVD removal, or diagnostic testing) prompted CSF sampling, increasing the heterogeneity of the samples and potentially creating sampling bias. In addition, low cell counts from individual subjects further limit the generalizability of our results. Nevertheless, our study is one of very few single-cell or single-nucleus transcriptomic studies of cerebrospinal fluid for hemorrhagic brain disease, and substantially increases the data available in the literature. While we hypothesize that the single-nucleus approach has allowed us to capture difficult-to-detect neutrophil states, this approach does have drawbacks. Nuclei contain substantially fewer transcripts than do whole cells, potentially diminishing our ability to identify transcriptionally regulated pathways relevant to disease biology. However, even small nuclear transcriptomes have proven reliable for cell type classification in our study. While single-cell transcriptomic methods are unlikely to be translatable directly to clinical diagnostics, they may generate candidates for the development of flow cytometry panels. We provide a proof-of-concept for this here, but with too few subjects to demonstrate the utility of these markers for diagnostic or prognostic purposes.

An intriguing question is whether the peripheral and CSF leukocyte populations diverge over time in intraventricular hemorrhage. At disease onset, rupture of blood vessels leads to deposition of blood in the brain and ventricles. Therefore, the blood and CSF leukocyte populations should be nearly identical at ictus. Bleeding usually stops over the course of hours, during which time the distinct environment of the CSF may induce changes in leukocytes that are different from those that occur in blood. In addition, the presence of blood and inflammatory material in the ventricles is likely to active migration of leukocytes into the CSF across the choroid plexus[47]. In a time series of single-cell RNA sequencing in blood and intracerebral hematoma of a single patient, Sansing and colleagues observe this manner of divergence[19]. After subarachnoid hemorrhage, differences in blood and CSF leukocyte populations have also been noted[34].

It would be valuable to extend the approaches we employed in this study to elucidate time-dependent changes in blood and CSF leukocytes across a larger cohort of patients in a variety of disease contexts — including intracerebral hemorrhage, aneurysmal subarachnoid hemorrhage, traumatic brain injury, and others. The

dynamics of these populations over time may have important implications for the development of common complications in these disorders. For example, post-hemorrhagic hydrocephalus is thought to arise, at least in part, from inflammatory stimulation of the choroid plexus. This prompts the question of whether a detailed understanding of leukocyte subpopulations in the CSF could help to predict which patients are likely to suffer persistent hydrocephalus after intraventricular hemorrhage. This would have important clinical implications for the timing of surgical interventions and may also shed light on modifiable molecular mechanisms for the treatment of post-hemorrhagic hydrocephalus.

Taken together, our results provide the most comprehensive cellular atlas of the CSF in IVH to date. This atlas reveals a rich diversity of cellular populations, including myeloid states not previously described in the central nervous system, including interferon-responsive neutrophils. We have further demonstrated that transcriptional markers from these populations can in many cases be validated at a protein level with flow cytometry. We anticipate that these results will set the stage for larger studies that elucidate the relevance of specific leukocyte subtypes to disease severity, progression, and outcome. Eventually, this will yield new diagnostic tools and therapeutic targets for intraventricular hemorrhage, a common, catastrophic disease with few effective treatments.

Figure Legends

Figure 1. Clinical characteristics of study participants. A. Study design. B. Computed tomography (CT) scans. Axial images (slice thickness=3 mm) from the first CT study obtained after EVD placement for a subject with ICH (i,ii) and SAH (iii, iv). B. Thalamic ICH with IVH most prominent in right lateral ventricle (RLV) and ventriculomegaly consistent with hydrocephalus (HC), with EVD visible in left lateral ventricle. C. More caudal slice from same CT as in (A) showing IVH in the third ventricle (3V) and bilateral lateral ventricles (LVs). D. Aneurysmal SAH with small amount of IVH in bilateral LVs, with EVD visible at the foramen of Monro. E. More caudal slice from same CT as in (A) showing blood in the basal cisterns in classical aneurysmal SAH pattern, with dilated temporal horns consistent with HC. F. Cell proportions in ventricular CSF assessed by cytospin columns.

Figure 2. snRNA-seq of ventricular CSF after IVH. A. Uniform manifold approximation and projection (UMAP) plot for snRNA-seq of ventricular CSF (11,191 nuclei from seven study participants). B. Quality metrics comparing cell processing methods. C. Dot plot showing expression of canonical marker genes across cell types.

Figure 3. Neutrophil diversity in CSF after IVH. A. UMAP indicating neutrophil subtypes. B. Annotation of neutrophil subtypes by scoring with marker genes from neutrophil subtypes identified in the blood[16]. C. Gene co-expression modules differentially expressed across neutrophil subtypes. ANOVA with post-hock TukeyHSD used for statistical significance testing (see **Table S8**). Post-hoc TukeyHSD *$p < 0.05$, **$p < 0.01$, ***$p < 0.001$, ****$p < 0.0001$.

Figure 4. Monocyte diversity in CSF after IVH. A. UMAP indicating monocyte subtypes. B. Annotation of monocyte subtypes by scoring with marker genes from select subtypes identified in a meta-analysis of monocytes and macrophages from healthy and diseased samples (MoMac)[31]. C. Gene co-expression modules differentially expressed across monocyte subtypes. Associated statistical significance testing (ANOVA with post-hoc Tukey HSD) is shown in **Supplemental Table 8**.

Figure 5. Lymphocyte diversity in the ventricular CSF. A. UMAP showing reference annotations in blood from the Azimuth data set[26]. B. Annotation of lymphocyte subtypes in CSF after IVH based on label transfer analysis. (C.,D.) Dot plots showing expression of marker genes in the reference set (C) and our lymphocyte population in CSF after IVH (D).

Figure 6. Flow cytometry of CSF after IVH. Aggregate data from n=3 samples from n=2 patients is shown, for a total of 72,725 events. A. Gating strategy for identifying the singlet, live, $CD45^+$ cell population (53,424 events) with CD3 and CD14 used to distinguish neutrophils (orange), monocytes (blue), and lymphocytes (green). Back gating onto the SSC-A vs. CD45 plot shows separation of these populations based on the characteristic distribution of these cells types by side scatter. B. Neutrophil population is further gated by CD10 and CD62L. Each quadrant is subsequently gated by either CD16b, CXCR1, or CXCR2. C. Monocyte population is further gated by CD62L and CD163. Each quadrant is subsequently gated by CXCR1.

Supplementary Figure S1. UMAPs of ventricular CSF colored by quality metrics. UMAPs of snRNA-seq of ventricular CSF (11,191 nuclei from seven study participants) colored by A. Preservation method. B. RNA Counts. C. Percentage Mitochondrial Counts.

Supplementary Figure S2. UMAPs of the neutrophil subset colored by quality metrics. UMAPs of snRNA-seq of the neutrophil subset colored by A. Preservation method. B. RNA Counts. C. Percentage Mitochondrial Counts.

Supplementary Figure S3. Annotation of neutrophil subtypes. Violin plots of neutrophil subtypes scored by marker genes from cell states found in blood during sepsis response[29].

Supplementary Figure S4. Gene co-expression Modules. All 12 modules differentially expressed across neutrophil subtypes.

Supplementary Figure S5. UMAPs of the monocyte subset colored by quality metrics. UMAPs of snRNA-seq of the monocyte subset colored by A. Preservation method. B. RNA Counts. C. Percentage Mitochondrial Counts.

Supplementary Figure S6. Annotation of monocyte subtypes. Violin plots of monocyte subtypes scored by marker genes from all the cell states found in the MoMac dataset[31].

Supplementary Figure S7. Gene co-expression Modules. All 14 modules differentially expressed across monocyte subtypes.

Supplementary Table S1. Markers for all cell types.

Supplementary Table S2. Markers for neutrophil states.

Supplementary Table S3. Neutrophil GCEC membership.

Supplementary Table S4. Neutrophil reference genes.

Supplementary Table S5. Markers for monocyte states.

Supplementary Table S6. Monocyte GCEC membership.

Supplementary Table S7. Monocyte reference genes.

Supplementary Table S8. Tests of significance (ANOVA+TukeyHSD) for gene list scores of the gene modules and references in neutrophils and monocytes (violin plots in Figures 3 and 4).

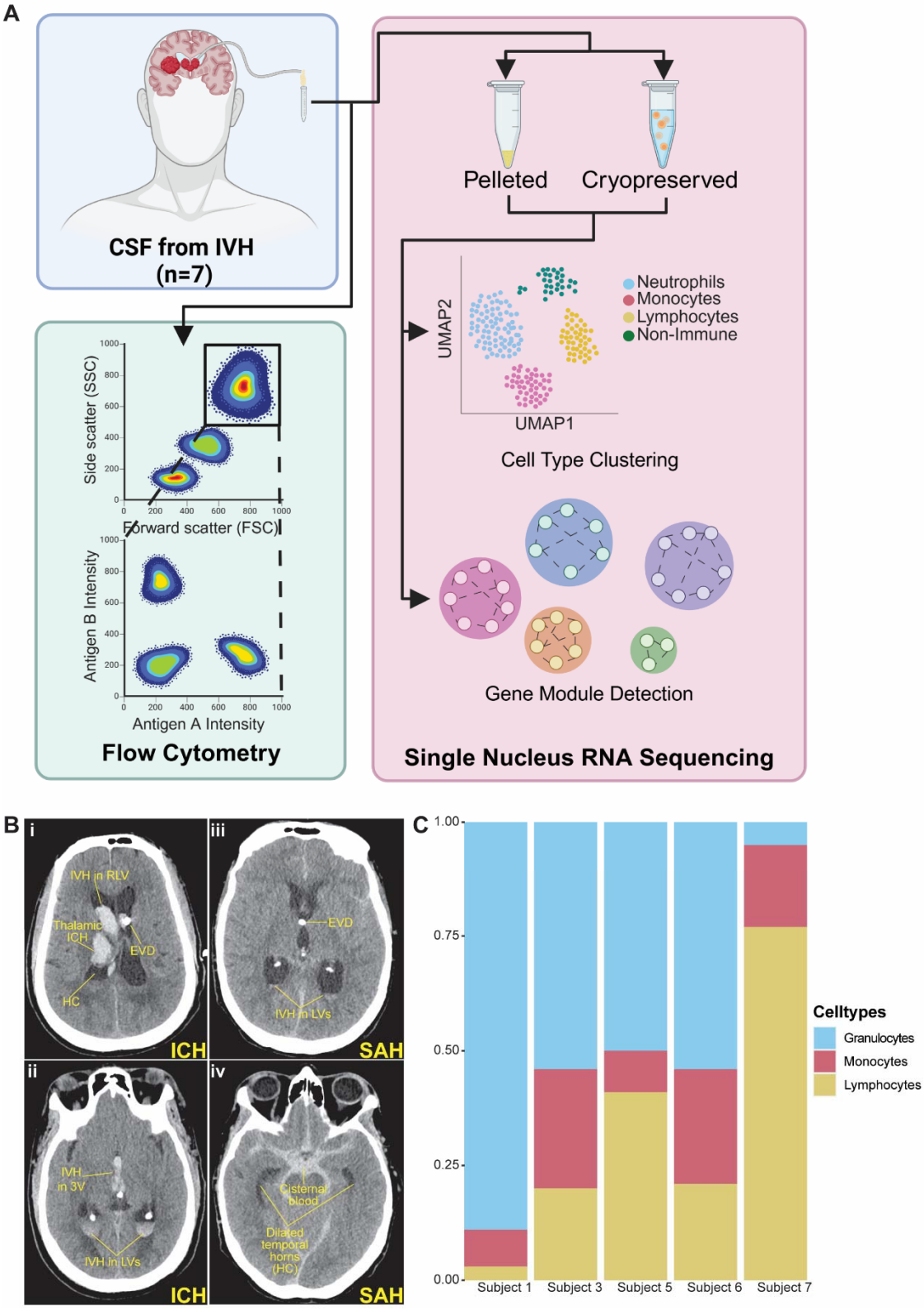
A
CSF from IVH
(n=7)
Pelleted
Cryopreserved
Side scatter (SSC)
Forward scatter (FSC)
Antigen B Intensity
Antigen A Intensity
Flow Cytometry
UMAP2
UMAP1
Neutrophils
Monocytes
Lymphocytes
Non-Immune
Cell Type Clustering
Gene Module Detection
Single Nucleus RNA Sequencing
B
i
IVH in RLV
Thalamic ICH
EVD
HC
ICH
iii
EVD
IVH in LVs
SAH
ii
IVH in 3V
IVH in LVs
ICH
iv
Cisternal blood
Dilated temporal horns (HC)
SAH
C
1.00
0.75
0.50
0.25
0.00
Subject 1
Subject 3
Subject 5
Subject 6
Subject 7
Celltypes
Granulocytes
Monocytes
Lymphocytes

Figure 1.

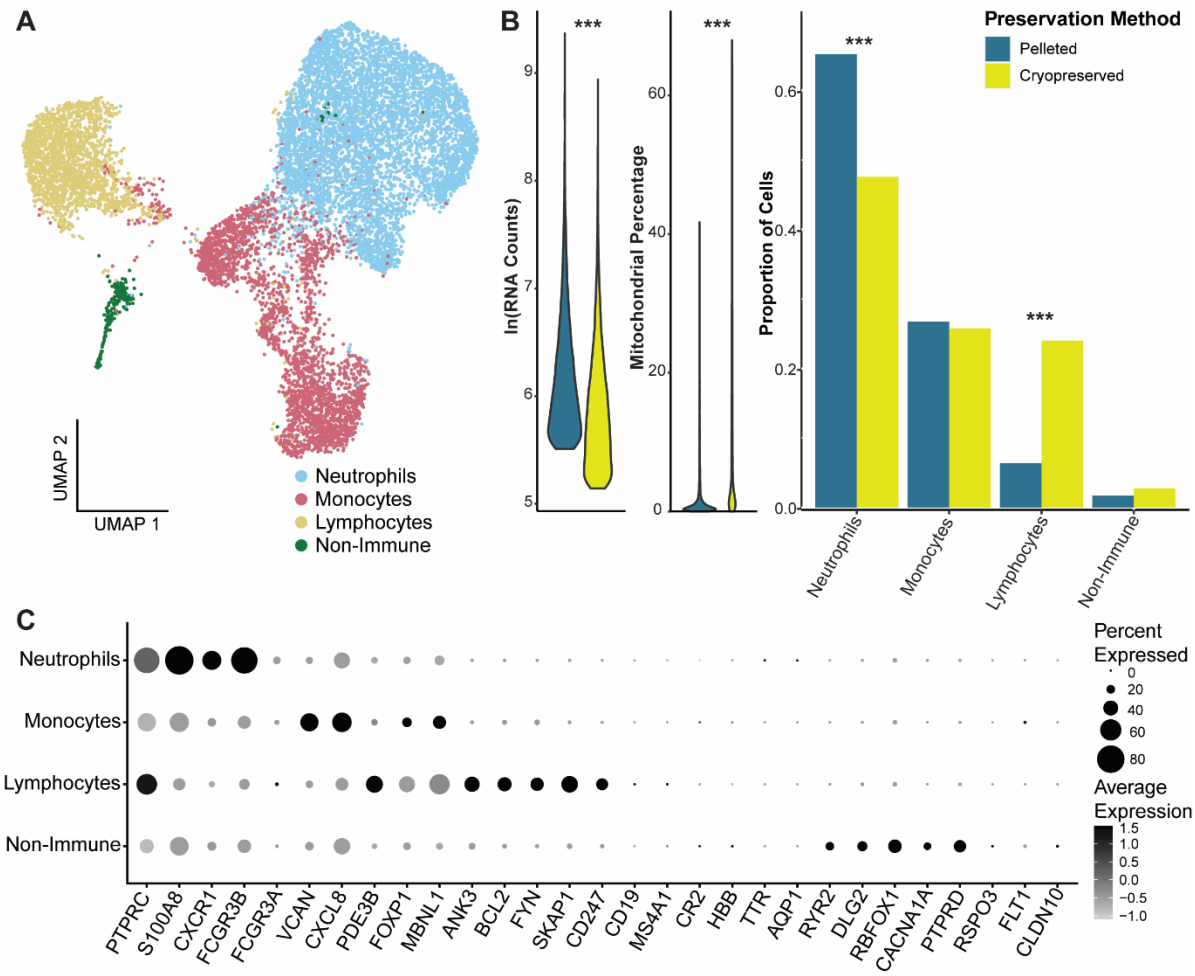
A
UMAP 2
UMAP 1
Neutrophils
Monocytes
Lymphocytes
Non-Immune
B
ln(RNA Counts)
Mitochondrial Percentage
Proportion of Cells
***
Preservation Method
Pelleted
Cryopreserved
Neutrophils
Monocytes
Lymphocytes
Non-Immune
C
Percent Expressed
Average Expression
PTPRC
S100A8
CXCR1
FCGR3B
FCGR3A
VCAN
CXCL8
PDE3B
FOXP1
MBNL1
ANK3
BCL2
FYN
SKAP1
CD247
CD19
MS4A1
CR2
HBB
TTR
AQP1
RYR2
DLG2
RBFOX1
CACNA1A
PTPRD
RSPO3
FLT1
CLDN10

Fig. 2

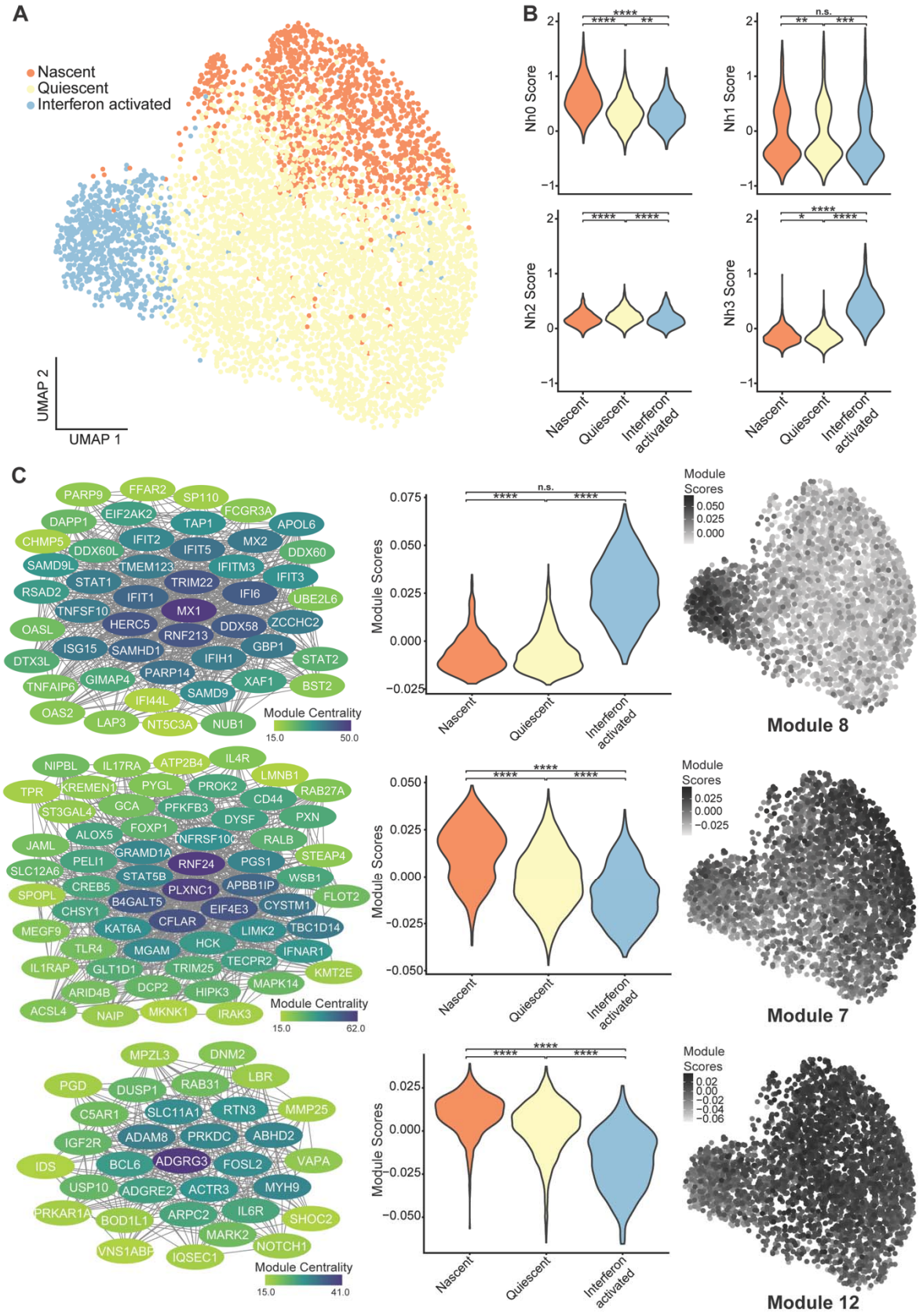
A
Nascent
Quiescent
Interferon activated
UMAP 2
UMAP 1
B
Nh0 Score
Nh1 Score
Nh2 Score
Nh3 Score
Nascent
Quiescent
Interferon activated
C
Module Centrality
Module Scores
Module 8
Module 7
Module 12

Fig. 3

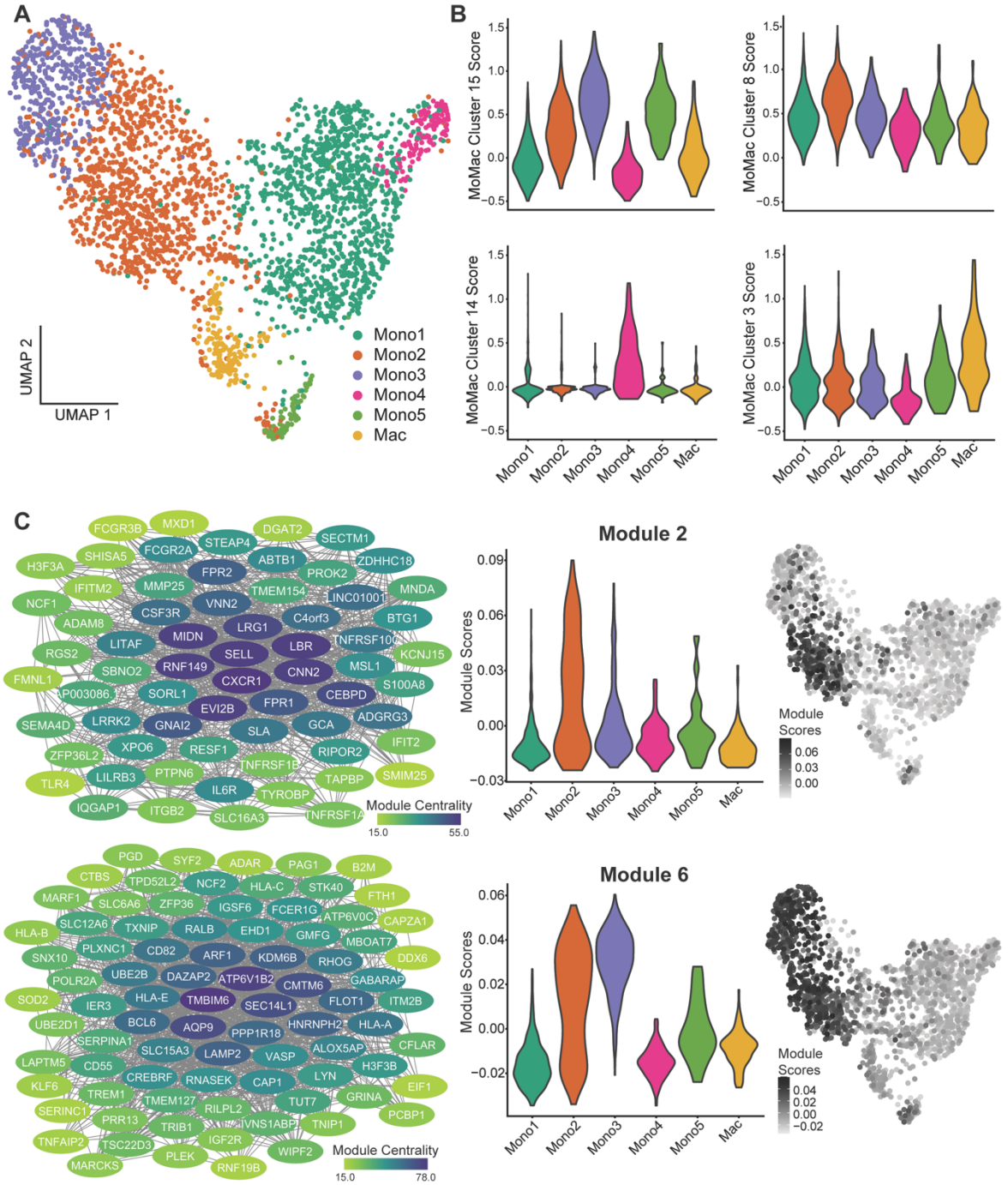
A
UMAP 2
UMAP 1
Mono1
Mono2
Mono3
Mono4
Mono5
Mac
B
MoMac Cluster 15 Score
MoMac Cluster 8 Score
MoMac Cluster 14 Score
MoMac Cluster 3 Score
C
Module 2
Module Scores
Module Centrality
15.0
55.0
Module 6
Module Scores
Module Centrality
15.0
78.0

Fig. 4

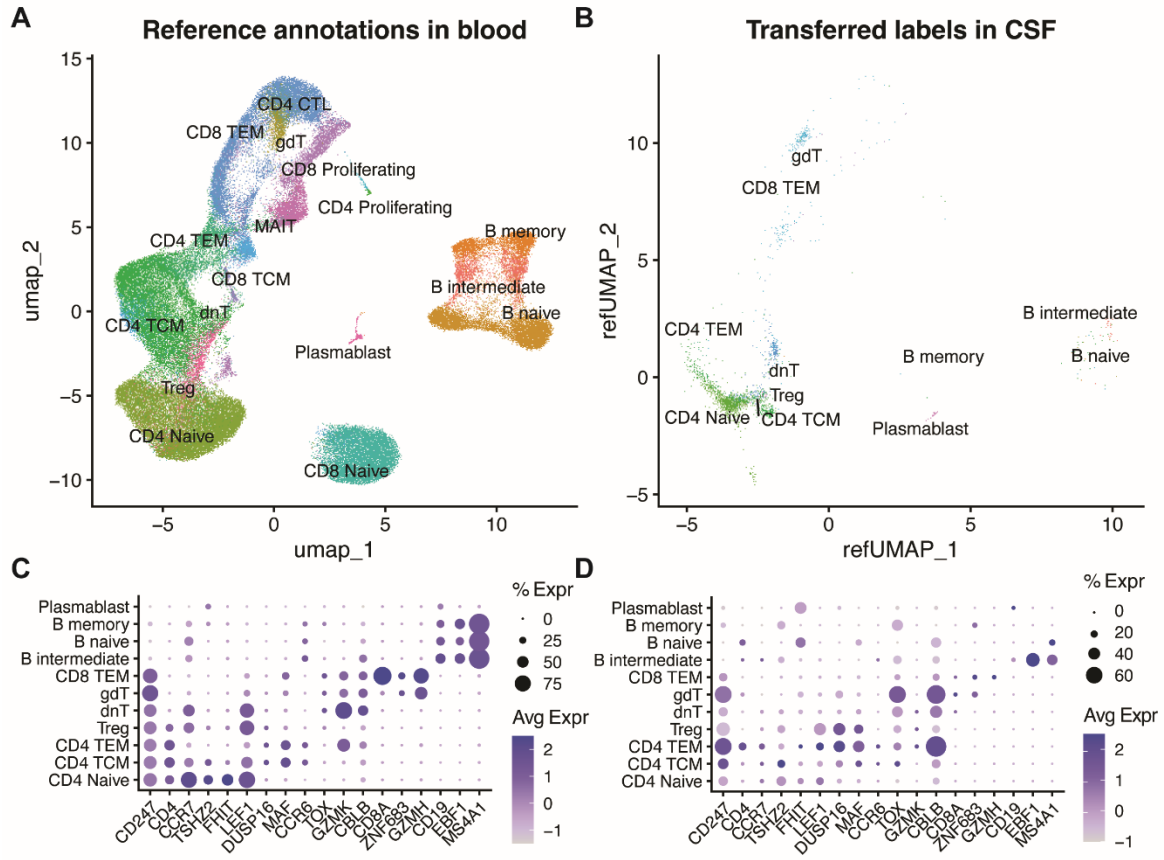
A
Reference annotations in blood
CD4 CTL
CD8 TEM
gdT
CD8 Proliferating
CD4 Proliferating
MAIT
CD4 TEM
B memory
CD8 TCM
B intermediate
dnT
B naive
CD4 TCM
Plasmablast
Treg
CD4 Naive
CD8 Naive
umap_1
umap_2
B
Transferred labels in CSF
gdT
CD8 TEM
B intermediate
CD4 TEM
B memory
B naive
dnT
Treg
CD4 Naive
CD4 TCM
Plasmablast
refUMAP_1
refUMAP_2
C
D
% Expr
Avg Expr
Plasmablast
B memory
B naive
B intermediate
CD8 TEM
gdT
dnT
Treg
CD4 TEM
CD4 TCM
CD4 Naive
CD247
CD4
CCR7
TSHZ2
FHIT
LEF1
DUSP16
MAF
CCR6
TOX
GZMK
CBLB
CD9A
ZNF683
GZMH
CD19
EBF1
MS4A1

Fig. 5

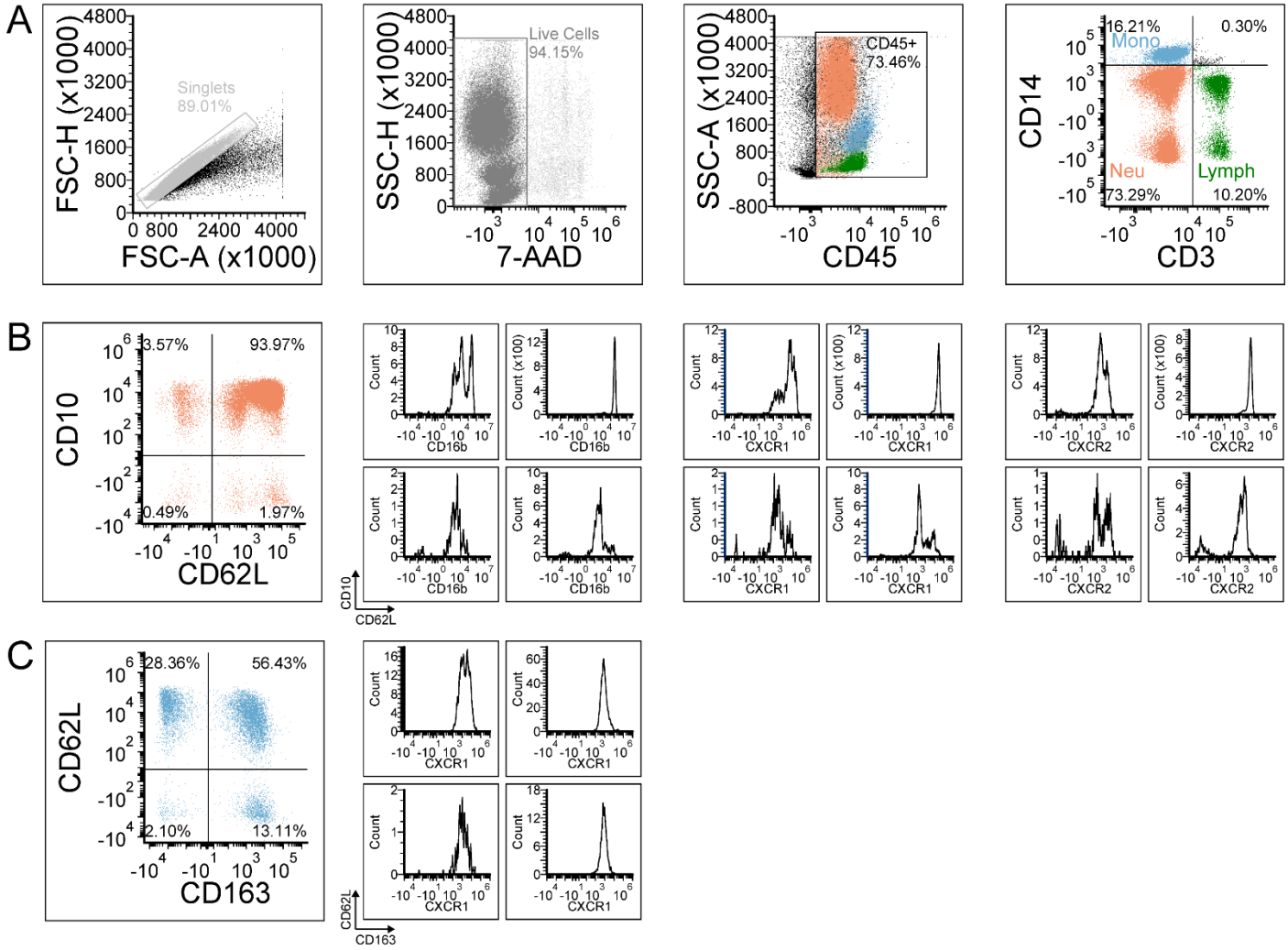
A
FSC-H (x1000)
FSC-A (x1000)
Singlets
89.01%
SSC-H (x1000)
7-AAD
Live Cells
94.15%
SSC-A (x1000)
CD45
CD45+
73.46%
CD14
CD3
16.21%
Mono
0.30%
Neu
73.29%
Lymph
10.20%
B
CD10
CD62L
3.57%
93.97%
0.49%
1.97%
Count
CD16b
Count (x100)
CXCR1
CXCR2
C
CD62L
CD163
28.36%
56.43%
2.10%
13.11%

Fig. 6.

Table 1. Clinical Characteristics.		
Characteristic	**ICH (N=6)**	**SAH (N=1)**
Patient Demographics		
Age — Median (Range)	57.5 (46-74)	75 (75)
Sex		
M	6	0
F	0	1
Race		
Black	3	0
White	2	1
Other	1	0
Pre-Hospital mRS — Median (Range)	0 (0-3)	1 (1)
Clinical Presentation		
Admission Glasgow Coma Scale		
13-15	1	1
9-12	0	0
3-8	5	0
ICH Score — Median (Range)*	2.5 (2-3)	-
Hunt-Hess Grade†	-	3
Modified Fisher Grade†	-	3
Hemorrhage Location		
Lobar	1	0
Deep	4	0
Infratentorial	1	0
Subarachnoid	0	1
IVH Present at Admission		
Yes	5	1
No	1‡	0
Etiology		
Hypertension	3	0
Hypertension + Coagulopathy	1	0
Anticoagulation	1	0
Aneurysm	0	1
Unknown	1	0
Sample Characteristics		
Post-Bleed Day at Time of CSF Collection - Median (Range)	12.5 (2-22)	17 (17)
Reason for CSF Collection		
EVD Insertion	1	0
Fever Evaluation	2	0
EVD Removal	2	1
Hydrocephalus Treatment	1	0

*Applicable only to ICH

†Applicable only to SAH

‡IVH not present on initial CT, but observed in left lateral ventricle on subsequent CT and MRI prior to CSF collection

Table 1.

References

1. Gaberel, T., Magheru, C. & Emery, E. Management of non-traumatic intraventricular hemorrhage. *Neurosurg Rev* **35**, 485–494; discussion 494-495 (2012).
2. Ziai, W. C. *et al.* Occurrence and impact of intracranial pressure elevation during treatment of severe intraventricular hemorrhage. *Crit Care Med* **40**, 1601–1608 (2012).
3. Bhattathiri, P. S., Gregson, B., Prasad, K. S. M., Mendelow, A. D., & STICH Investigators. Intraventricular hemorrhage and hydrocephalus after spontaneous intracerebral hemorrhage: results from the STICH trial. *Acta Neurochir Suppl* **96**, 65–68 (2006).
4. Shah, V. A. *et al.* One-Year Outcome Trajectories and Factors Associated with Functional Recovery Among Survivors of Intracerebral and Intraventricular Hemorrhage With Initial Severe Disability. *JAMA Neurol* **79**, 856–868 (2022).
5. Lovasik, B. P. *et al.* The Effect of External Ventricular Drain Use in Intracerebral Hemorrhage. *World Neurosurg* **94**, 309–318 (2016).
6. Herrick, D. B. *et al.* Determinants of external ventricular drain placement and associated outcomes in patients with spontaneous intraventricular hemorrhage. *Neurocrit Care* **21**, 426–434 (2014).
7. Hanley, D. F. *et al.* Thrombolytic removal of intraventricular haemorrhage in treatment of severe stroke: results of the randomised, multicentre, multiregion, placebo-controlled CLEAR III trial. *Lancet* **389**, 603–611 (2017).
8. Akinduro, O. O. *et al.* Predictors of Ventriculoperitoneal shunting following Subarachnoid Hemorrhage treated with External Ventricular Drainage. *Neurocrit Care* **32**, 755–764 (2020).
9. Sadegh, C. *et al.* Choroid plexus-targeted NKCC1 overexpression to treat post-hemorrhagic hydrocephalus. *Neuron* **111**, 1591-1608.e4 (2023).
10. Karimy, J. K. *et al.* Inflammation-dependent cerebrospinal fluid hypersecretion by the choroid plexus epithelium in posthemorrhagic hydrocephalus. *Nat Med* **23**, 997–1003 (2017).
11. Garton, T. *et al.* Intraventricular Hemorrhage: the Role of Blood Components in Secondary Injury and Hydrocephalus. *Transl Stroke Res* **7**, 447–451 (2016).
12. Wang, Y. *et al.* Irisin ameliorates neuroinflammation and neuronal apoptosis through integrin αVβ5/AMPK signaling pathway after intracerebral hemorrhage in mice. *J Neuroinflammation* **19**, 82 (2022).
13. Shen, J. *et al.* Neurogenesis after primary intracerebral hemorrhage in adult human brain. *J Cereb Blood Flow Metab* **28**, 1460–1468 (2008).
14. Xiong, X.-Y. & Yang, Q.-W. Rethinking the roles of inflammation in the intracerebral hemorrhage. *Transl Stroke Res* **6**, 339–341 (2015).
15. Single-cell transcriptome profiling reveals neutrophil heterogeneity in homeostasis and infection - PubMed. https://pubmed.ncbi.nlm.nih.gov/32719519/.
16. Wigerblad, G. *et al.* Single-Cell Analysis Reveals the Range of Transcriptional States of Circulating Human Neutrophils. *J Immunol* **209**, 772–782 (2022).
17. Haruna, N.-F. *et al.* scRNA-seq profiling of human granulocytes reveals expansion of developmentally flexible neutrophil precursors with mixed neutrophil and eosinophil properties in asthma. *J Leukoc Biol* **116**, 1184–1197 (2024).
18. Xiao, H. *et al.* High-throughput sequencing unravels the cell heterogeneity of cerebrospinal fluid in the bacterial meningitis of children. *Front Immunol* **13**, 872832 (2022).
19. Goods, B. A. *et al.* Leukocyte dynamics after intracerebral hemorrhage in a living patient reveal rapid adaptations to tissue milieu. *JCI Insight* **6**, e145857, 145857 (2021).
20. Meng, N. *et al.* Single-cell transcriptomic landscape reveals the role of intermediate monocytes in aneurysmal subarachnoid hemorrhage. *Front Cell Dev Biol* **12**, 1401573 (2024).
21. Sanchez, S. *et al.* Modulation of the Immunological Milieu in Acute Aneurysmal Subarachnoid Hemorrhage: The Potential Role of Monocytes Through CXCL10 Secretion. *Transl Stroke Res* **16**, 88–95 (2025).
22. Uhlen, M. *et al.* A genome-wide transcriptomic analysis of protein-coding genes in human blood cells. *Science* **366**, eaax9198 (2019).
23. Karlsson, M. *et al.* A single-cell type transcriptomics map of human tissues. *Sci Adv* **7**, eabh2169 (2021).
24. The Human Protein Atlas. https://www.proteinatlas.org/.
25. Wildermuth, E. *et al.* A single-cell genomic atlas for the effects of chronic ethanol exposure in the mouse dorsal striatum. *Mol Psychiatry* (2025) doi:10.1038/s41380-025-03014-z.
26. Hao, Y. *et al.* Integrated analysis of multimodal single-cell data. *Cell* **184**, 3573-3587.e29 (2021).
27. Gungabeesoon, J. *et al.* A neutrophil response linked to tumor control in immunotherapy. *Cell* **186**, 1448-1464.e20 (2023).
28. Sinha, S. *et al.* Dexamethasone modulates immature neutrophils and interferon programming in severe COVID-19. *Nat Med* **28**, 201–211 (2022).
29. Kwok, A. J. *et al.* Neutrophils and emergency granulopoiesis drive immune suppression and an extreme response endotype during sepsis. *Nat Immunol* **24**, 767–779 (2023).

30. Siakaeva, E. *et al.* Neutrophil Maturation and Survival Is Controlled by IFN-Dependent Regulation of NAMPT Signaling. *Int J Mol Sci* **20**, 5584 (2019).
31. Mulder, K. *et al.* Cross-tissue single-cell landscape of human monocytes and macrophages in health and disease. *Immunity* **54**, 1883-1900.e5 (2021).
32. Wong, K. L. *et al.* Gene expression profiling reveals the defining features of the classical, intermediate, and nonclassical human monocyte subsets. *Blood* **118**, e16–e31 (2011).
33. Jiang, C. *et al.* Immune changes in peripheral blood and hematoma of patients with intracerebral hemorrhage. *FASEB J* **34**, 2774–2791 (2020).
34. Moraes, L. *et al.* Immune cells subpopulations in cerebrospinal fluid and peripheral blood of patients with Aneurysmal Subarachnoid Hemorrhage. *Springerplus* **4**, 195 (2015).
35. Glatzel, A. *et al.* Patterns of chemokine receptor expression on peripheral blood gamma delta T lymphocytes: strong expression of CCR5 is a selective feature of V delta 2/V gamma 9 gamma delta T cells. *J Immunol* **168**, 4920–4929 (2002).
36. Grieshaber-Bouyer, R. & Nigrovic, P. A. Neutrophil Heterogeneity as Therapeutic Opportunity in Immune-Mediated Disease. *Front Immunol* **10**, 346 (2019).
37. Kamp, V. M. *et al.* Human suppressive neutrophils CD16bright/CD62Ldim exhibit decreased adhesion. *J Leukoc Biol* **92**, 1011–1020 (2012).
38. Askenase, M. H. *et al.* Longitudinal transcriptomics define the stages of myeloid activation in the living human brain after intracerebral hemorrhage. *Sci Immunol* **6**, eabd6279 (2021).
39. Pak, C. B., Imanishi, J., Kishida, T. & Matsuo, A. Increased nitroblue tetrazolium dye reduction by human neutrophils stimulated by interferon in vitro. *Microbiol Immunol* **24**, 717–723 (1980).
40. Chen, X. *et al.* Expression of costimulatory TNFR2 induces resistance of CD4+FoxP3- conventional T cells to suppression by CD4+FoxP3+ regulatory T cells. *J Immunol* **185**, 174–182 (2010).
41. Seo, S.-U. *et al.* Type I Interferon Signaling Regulates Ly6Chi Monocytes and Neutrophils during Acute Viral Pneumonia in Mice. *PLOS Pathogens* **7**, e1001304 (2011).
42. Nandi, B. & Behar, S. M. Regulation of neutrophils by interferon-γ limits lung inflammation during tuberculosis infection. *J Exp Med* **208**, 2251–2262 (2011).
43. Benguigui, M. *et al.* Interferon-stimulated neutrophils as a predictor of immunotherapy response. *Cancer Cell* **42**, 253-265.e12 (2024).
44. Thomas, A. J., Ogilvy, C. S., Griessenauer, C. J. & Hanafy, K. A. Macrophage CD163 expression in cerebrospinal fluid: association with subarachnoid hemorrhage outcome. *J Neurosurg* **131**, 47–53 (2019).
45. de Graaf, M. T. *et al.* Central memory CD4+ T cells dominate the normal cerebrospinal fluid. *Cytometry B Clin Cytom* **80**, 43–50 (2011).
46. Kivisäkk, P. *et al.* Human cerebrospinal fluid central memory CD4+ T cells: evidence for trafficking through choroid plexus and meninges via P-selectin. *Proc Natl Acad Sci U S A* **100**, 8389–8394 (2003).
47. Xu, H. *et al.* The choroid plexus synergizes with immune cells during neuroinflammation. *Cell* **187**, 4946-4963.e17 (2024).